ELSEVIER

BRACHYTHERAPY

Brachytherapy 19 (2020) 544–553

Physics

Advanced design, simulation, and dosimetry of a novel rectal applicator for contact brachytherapy with a conventional HDR ^{192}Ir source

Murillo Bellezzo[1,2], Gabriel P. Fonseca[1], Robert Voncken[1], An-Sofie Verrijssen[1], Celine Van Beveren[1], Erik Roelofs[1], Hélio Yoriyaz[2], Brigitte Reniers[3], Evert J. Van Limbergen[1], Maaike Berbée[1], Frank Verhaegen[1,*]

[1]*Department of Radiation Oncology (MAASTRO), GROW School for Oncology and Developmental Biology, Maastricht University Medical Center, Maastricht, The Netherlands*

[2]*Centro de Engenharia Nuclear, Instituto de Pesquisas Energéticas e Nucleares IPEN-CNEN/SP, São Paulo, Brazil*

[3]*Research group NuTeC, Centre for Environmental Sciences, Hasselt University, Diepenbeek, Belgium*

ABSTRACT

PURPOSE: Dose escalation yields higher complete response to rectal tumors, which may enable the omission of surgery. Dose escalation using 50 kVp contact x-ray brachytherapy (CXB) allow the treatment of a selective volume, resulting in low toxicity and organs-at-risk preservation. However, the use of CXB devices is limited because of its high cost and lack of treatment planning tools. Hence, the MAASTRO applicator (for HDR ^{192}Ir sources) was developed and characterized by measurements and Monte Carlo simulations to be a cost-effective alternative to CXB devices.

METHODS AND MATERIALS: A cylindrical applicator with lateral shielding was designed to be used with a rectoscope using its tip as treatment surface. Both the applicator and the rectoscope have a slanted edge to potentially allow easier placement against tumors. The applicator design was achieved by Monte Carlo modeling and validated experimentally with film dosimetry, using the Papillon 50 (P50) device as reference.

RESULTS: The applicator delivers CXB doses in less than 9 min using a 20375 U source for a treatment area of approximately 20 × 20 mm^2 at 2 mm depth. Normalized at 2 mm, the dose falloff for depths of 0 mm, 5 mm, and 10 mm are 130%, 70%, and 43% for the P50 and 140%, 67%, and 38% for the MAASTRO applicator, respectively.

CONCLUSIONS: The MAASTRO applicator was designed to use HDR ^{192}Ir sources to deliver a dose distribution similar to those of CXB devices. The applicator may provide a cost-effective solution for endoluminal boosting with clinical treatment planning system integration. © 2020 Published by Elsevier Inc. on behalf of American Brachytherapy Society.

Keywords: Brachytherapy; Monte Carlo; Contact radiotherapy; Rectal applicator

Introduction

Colorectal cancer is the third most commonly diagnosed type of cancer in the United States for both men and women, with approximately one hundred fifty thousand new cases estimated for the year of 2019, with nearly one-third of these cases located in the rectum (1). The main curative treatment for rectal cancer is surgical resection of the tumor along with part of the rectum and surrounding fat, which may result in long-term morbidity (2). Depending on the anticipated risk of a recurrence, patients may receive neoadjuvant (chemo) radiotherapy. Between 15% and 20% of these patients show a complete response after chemoradiotherapy. In these patients,

Received 24 October 2019; received in revised form 30 March 2020; accepted 30 March 2020.

Conflict of interest: several co-authors are involved in a patent application for the applicator mentioned in the article.

Financial disclosure: M.B. was partially supported by CNPq, Conselho Nacional de Desenvolvimento Cientifico e Tecnologico e Brazil, grant number 200402/2015-3.

* Corresponding author. Department of Radiation Oncology (MAASTRO), GROW School for Oncology and Developmental Biology, Maastricht University Medical Center, 6201 BN Maastricht, The Netherlands. Tel.: +31-0-88-4455792; fax: 0031 88 44 55 667.

E-mail address: frank.verhaegen@maastro.nl (F. Verhaegen).

1538-4721/$ - see front matter © 2020 Published by Elsevier Inc. on behalf of American Brachytherapy Society.
https://doi.org/10.1016/j.brachy.2020.03.009

surgery can be omitted. Radiation dose escalation to the tumor appears to increase the chance of a complete response and thereby the chance of organ preservation (3). Advantages of endoluminal boosting techniques, such as contact x-ray brachytherapy (CXB) using 50 kVp X-rays, include the possibility of better targeting small volumes than external beam radiotherapy, providing preservation of organs at risk (OAR) and better toxicity profiles (4). However, the widespread use of CXB devices is restricted because of its high cost and lack of treatment planning tools. A previous study (5) showed that it is possible to develop a brachytherapy (BT) applicator (patent pending) that uses high-dose-rate (HDR) ^{192}Ir sources to generate a dose distribution similar to those generated by CXB devices. This offers a cost-effective solution for endoluminal boosting with the possibility of integration with currently available treatment planning systems (TPSs). The applicator had a cylindrical design with lateral shielding, positioning the source at multiple points perpendicular to the contact surface, and a steep dose falloff could be achieved by placing the sources close to the tumor due to the inverse square law. Nonetheless, the uncertainty on source positioning for current available afterloaders (±1.0 mm (6,7)) would directly affect the distance between the sources and the tumor, changing the dose distribution and dose falloff shapes. Moreover, having the source perpendicular to the tumor results in a lower dose rate than when the source is parallel and close to the tumor, requiring more lateral shielding to protect OAR. Furthermore, several discussions among experts in the field revealed that a straight edge on the applicator head would be less practical than a slanted-edge design. A slanted-edge design would simplify positioning the applicator on a tumor originating on the side wall. To solve all these problems, the original design was revised.

Hence, the present study presents the modeling and experimental validation of a new applicator prototype (MAASTRO applicator) that has been designed to position the source parallel to the tumor, providing a higher dose rate with lower dose leakage, and a dose distribution less susceptible to nonuniformity because of source position uncertainties.

Methods and materials

The MAASTRO applicator (patent pending) is under development in a partnership between MAASTRO (Maastricht, NL) and Varian Medical Systems (CA), who codeveloped the prototype of the applicator and proctoscope for experimental validation. The experimental validation, however, was performed with a simplified model of a proctoscope to reduce experimental uncertainties (see Experimental Validation section). Finally, the dose distribution based on the CAD model of the applicator (with a complete proctoscope and small dimension changes due to manufacturing restrictions—see Simulation of the Virtual Model of the Applicator section) was simulated with Monte Carlo (MC).

Design of the MAASTRO applicator

The MAASTRO applicator was designed to have a dose falloff similar to the one generated by the CXB Papillon 50 (P50) device (Ariane Medical Systems, Derbyshire, UK) (8,9), delivering at least 30 Gy for a region not smaller than 20×20 mm^2 at the applicator contact surface (contact surface shown in Fig. 1a). This is a typical CXB treatment dose (10,11), which can be delivered under 9 min with the MAASTRO applicator when using a source with air kerma strength of 20375 U (representing the lowest dose rate, when the source is expected to be replaced), and a field size (90% isodose) of approximately 20×20 mm^2 at 2 mm depth.

The applicator was designed with a cylindrical shape to be used with a proctoscope that has two main functions: to allow visually guided positioning against rectal wall tumors using its tip as contact surface, and to provide lateral shielding to preserve OAR. The design of the MAASTRO applicator is presented in Fig. 1. Figure 1a shows the channel arrangement inside the applicator with the contact surface highlighted, whereas Fig. 1b shows a top view of the applicator. Figure 1c shows a cross-section (along the dashed line of Fig. 1b) of the applicator inserted into the proctoscope, and an inset with a perpendicular view of the contact surface.

Both the applicator and the proctoscope have a slanted edge of 50° (Fig. 1c) to allow the channels to bend with a minimum radius of 13 mm, placing them parallel to most of the contact surface. The slanted edge also increases the contact surface without increasing the applicator diameter and, it is believed that it may provide a better placement of the applicator against tumors.

Several designs were studied to find a channel arrangement that would result in a homogeneous dose distribution between 1 mm and 2 mm depth from the applicator surface. Setups with multiple straight channels following the elliptical surface (similar design as (5)) would have the same problems pointed out in the introduction, and channels emerging from the center and curved toward the applicator edges would create a small treatment region. Hence, the best channel arrangement found to cover the contact surface has two elliptical arcs adjoining the edges of the contact surface (outermost channels of Fig. 1b) and three central channels, as presented in Figs. 1a and 1b. Such an arrangement places most part of the channels parallel to the contact surface, resulting in a distance of 2.50 ± 0.15 mm between the center of the channel and the contact surface (as shown in Fig. 1c). This is an advantage when compared with the previous applicator model (5), in which the sources were positioned perpendicular to the contact surface, resulting in a distance uncertainty of ±1.0 mm due to the afterloader precision.

Such an arrangement of the channels, however, does not uniformly cover the contact surface because the most distal source dwell position for each channel does not reach the

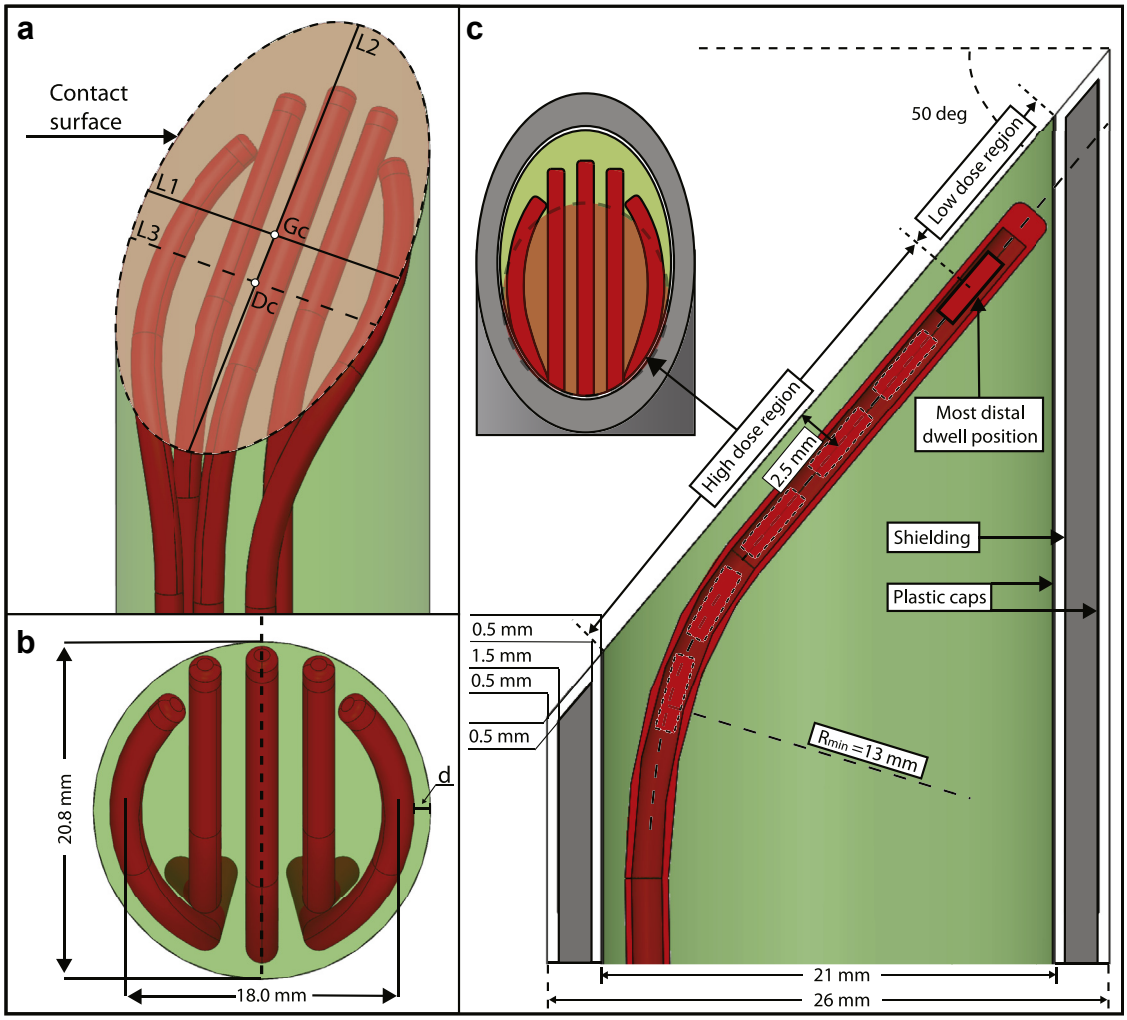

Fig. 1. Model of the MAASTRO applicator prototype used for experimental validation. (a) Isometric view of the applicator with the contact surface highlighted. The contact surface geometric center (Gc) is represented by the intersection between lines L1 and L2. However, because the most distal dwell positions of each channel do not reach the edge of the applicator, a shift is anticipated between Gc and the center of the dose distribution (Dc), represented by the intersection between lines L2 and L3; (b) Top view of the applicator, showing that there is a minimum distance (d) of approximately 0.5 mm between the catheter and the lateral wall of the applicator because the channel (not shown) to guide the catheter is slightly thicker than the catheter and there is also a minimum wall thickness that can be 3D printed, resulting in an applicator with 20.8 mm diameter core with a maximum distance of 18 mm between the side catheters along the smaller diameter of the contact surface and; (c) Cross-section along dashed line on b of the applicator inserted into the proctoscope, with a inset showing a perpendicular view of the contact surface, highlighting its high-dose region. The proctoscope has a 1.5 mm-thick tungsten alloy (Inermet IT180, $\rho = 18.0$ g/cm^3) shielding encapsulated by 0.5 mm-thick plastic caps. This is carried out to avoid corrosion of the shielding and stop secondary electrons.

sharp edge of the applicator, as shown in Fig. 1c, resulting in a low-dose region close to the edge far of the applicator. The high-dose region of the contact surface is highlighted in the inset of Fig. 1c (note that its exact dimensions and shape will change according to the designed treatment plan). Hence, there is an anticipated shift between the geometric center of the contact surface (Gc of Fig. 1a) and the center of the dose distribution (Dc of Fig. 1a).

Despite the fact that part of the contact surface delivers a lower dose, the high-dose region has approximately the same size as an applicator with a straight edge and sources perpendicular to the contact surface. However, placing the channels parallel to the contact surface provides a greater dose rate, lower dose leakage, and lower uncertainty on the distance between the source and the contact surface.

A disadvantage could be that the low-dose region on the contact surface holds a risk of undertreating the target volume. To solve this problem and guide the positioning of the applicator against the tumor considering the high- and low-dose regions, clearly visible markings will be engraved at the interior of the proctoscope.

Treatment planning and Monte Carlo simulations

Treatment planning

Two treatment plans were created for experimental validation of the applicator prototype. Plans were created using the TPS BrachyVision v15 (Varian Medical Systems) based on CT images of the applicator with 0.1 mm resolution acquired with an X-RAD 225Cx system (Precision X-Ray Inc., CT).

Both plans had interdwell distances of 2 mm for all the channels; however, one plan had fixed dwell times of 1 s for all dwell positions (created to verify dwell positions), whereas a second plan was optimized to have a dose flatness of ±2% at 2 mm depth, resulting in a treatment region (90% isodose) of an approximately square 20 × 20 mm^2 in water (it is not possible to have a uniform dose distribution at the contact surface because of the proximity to the channels).

All experiments (and CT images acquisition) were performed using the 3D-printed applicator core (which was printed in a single piece). However, the proctoscope was printed in multiple parts to encapsulate the shielding. This led to an increase in the geometric uncertainty and did not allow the applicator contact surface to be flush with the irradiated surface. Therefore, a simplified version of the proctoscope (containing only the shielding piece) was used for experimental validation of the MC simulations. Once the MC simulations were validated, a third treatment plan was created based on the CAD model of the applicator and proctoscope to simulate the expected dose distribution for the applicator with the complete proctoscope. The final model of the applicator is expected to be very similar to the simulated CAD model, nonetheless, the applicator will be commissioned before clinical trials.

Monte Carlo simulations

MC is currently the gold standard for particle transport simulations. Hence, MC simulations were used as reference for the experimental validation. The MC code MCNP6.1 (12) was used for all simulations in this study, using a model for the GammaMed Plus HDR ^{192}Ir source that was previously validated (5) against TG-43 (13) dose data available in the literature (14).

Dose distributions were scored in virtual grids as dose-to-water-in-medium ($D_{w,m}$) (15) using track length scoring (16) without electron transport. Electron transport was simulated only to evaluate the dose leakage of the virtual model of the applicator. The MC parameters used for the first set of simulations (experimental validation of the applicator prototype) are summarized in Table 1 and the MC parameters for the second set of simulations (based on the CAD model of the applicator) are summarized in Table 2. Both tables are in the Appendix.

Experimental validation

The applicator and plastic parts of the proctoscope produced for experimental validation were both 3D printed by Varian Medical Systems using stereolithography technology. However, small geometric variations (0.1–0.2 mm) are inherent of 3D-printed models, especially in the case of the proctoscope, that was printed in multiple pieces to encapsulate the tungsten alloy shielding (which was not 3D printed). Hence, the experimental validation of the prototype was performed without the proctoscope to mitigate experimental uncertainties. Only the applicator with a diameter of 20.8 mm and a 1.5 mm-thick shielding made of tungsten alloy (Inermet IT180 (17), ρ = 18.0 g/cm^3–95.0% W, 2.5% Ni and 2.5% Cu) with internal diameter of 21 mm was used.

The experimental validation consisted of two main stages: source position verification and film dosimetry.

Source position verification

Source position verification was performed using the Iridium Imaging System (IrIS—patent pending). The working principle for applicator commissioning using the IrIS system was thoroughly described by Fonseca *et al.* (18). It uses the radiation emitted by the BT source to acquire a projection of the applicator into an IP and later it sends the source inside the applicator and registers the dwell positions by applying a 2D Gaussian fit to the IP response and compare them with the treatment plan. The IP used by Fonseca *et al.* had a pixel size of 0.4 mm and the uncertainty to define the dwell positions was estimated in 0.2 mm. The IP used in the present study was the PaxScan 2530 HE (Varex, Salt lake City, UT), which has a pixel size of 0.14 mm and time resolution of up to 0.03 s; therefore, the uncertainty to determine the dwell positions is most likely lower than previously reported.

The adopted plan had dwell times of 1 s and interdwell distances of 2 mm, with the source trajectory initially defined following the center of each channel. As the results are shown in real time, it is possible to adjust the treatment plan on the TPS to follow the source trajectory measured experimentally because the source does not follow the center of a curved channel, especially for channels with a small curvature radius as those in the MAASTRO applicator. Once the measured source trajectory matches the trajectory on the TPS, the applicator model on the TPS is properly adjusted and other treatment plans can be adopted. The number of dwell positions per channel ranged from 11 to 14 and the mean deviation from the planned dwell position was averaged over five measurements per channel (performed after source path optimization).

Film dosimetry

There were two experimental setups adopted to validate the MC simulations using film dosimetry, one to evaluate the dose distribution at different depths in solid water and a second one to evaluate dose leakage around the shielding. Both setups are shown in Fig. 2.

Gafchromic EBT-XD films (IPS Technologies, NJ), lot 05081804 were used for both experiments because of theirs extended dose range (0.1–60 Gy (19)), making it suitable to measure depth doses distributions (~15–30 Gy) and also regions with low dose leakage (less than 2 Gy). Films were calibrated between 0.25 and 50 Gy using the triple channel method (20) with a 6 MV photon beam (EBT-XD films have a low energy dependence (19,21)) from a Varian TrueBeam accelerator (Varian Medical Systems). Films were placed at the linear accelerator isocenter, between 5 cm of solid water (on top of the films to avoid the buildup region) and 20 cm

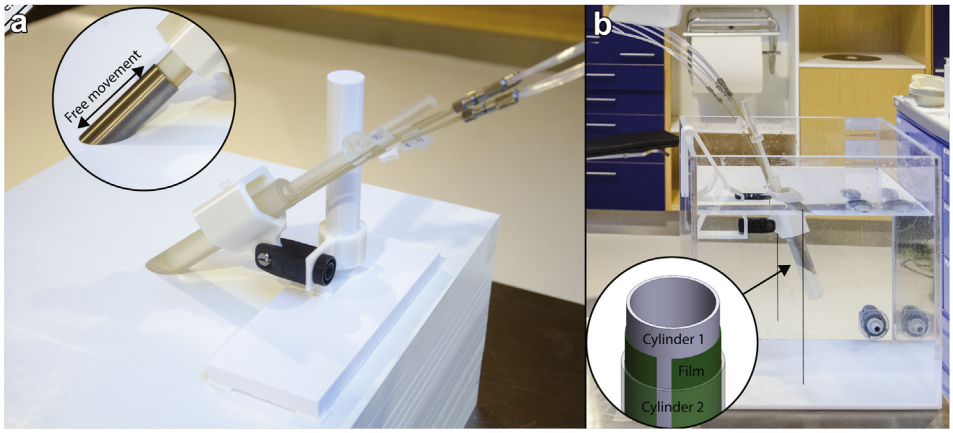

Fig. 2. (a) Experimental setup for dose measurement at different depths in solid water. The applicator was held in position by a 3D-printed holder with several degrees of freedom to ensure that the contact surface of the applicator was in contact with the solid water surface. Films were placed flat between 25 cm of solid water and a top solid water slab to define scoring depth. The shielding (inset) was purposely not fixed to the applicator, so it would be possible to shift it along the applicator to verify if the contact surface was flush with the solid water before putting the shielding back in position for irradiation. (b) Experiments for dose leakage measurements around the shielding were performed with the applicator axis slightly inclined from the vertical axis (~20°) to reduce transfer guide tubes curvature. The shielding was fixed around the applicator and the film was held between two concentric 3D-printed cylinders (inset) made of PLA (polylactic acid, $\rho = 1.2$ g/cm^3 – $(C_3H_4O_2)_n$), cylinder 1 would snugly fit around the shielding, defining the scoring distance, whereas the second cylinder would keep the film in place during irradiation.

of solid water under the films for backscattering using the PTW RW3 solid water phantom (PTW Freiburg GmbH, Breisgau, DE). Three films were irradiated separately for each dose of the calibration curve and scanned 24 h after irradiation in portrait mode using an EPSON (Nagano, JP) perfection V750 PRO scanner with 96 dpi resolution.

Depth dose distributions. The dose distribution was measured at 1 mm, 2 mm, and 5 mm depth in a PTW RW3 solid water phantom (PTW Freiburg GmbH, Breisgau, DE). Figure 2a shows the experimental setup to measure the dose distribution at different depths. Most dwell positions are 2.5 mm away from the contact surface (Fig. 1a, considering the source following the center of the channels), resulting in an intense dose gradient close to the applicator. To reduce experimental uncertainties, three separate films irradiations were performed at each scoring depth, placed flat between 25 cm of solid water and a top solid water slab of thickness of 1 mm, 2 mm, or 5 mm to define the scoring depth. Films were registered to each other using MATLAB (the MathWorks, Inc., MA), and the average dose distribution of the three films at the same depth was compared with the MC simulations that adopted a rectangular virtual grid with $0.2 \times 0.2 \times 0.025$ (film active layer thickness (19)) mm^3 voxel size for each scoring depth.

Experimental results were compared with MC simulations using isodoses, global dose ratios [(measured − simulated dose)/Ref. dose] and gamma analysis (22,23) with acceptance criteria of DD/DTA (3%/1 mm). The reference doses for the isodoses and global dose ratios were obtained from the MC simulations considering the center of the dose distribution at each depth.

Dose leakage. Dose leakage was measured with the tip of the applicator centralized inside a $36 \times 30 \times 34$ cm^3 water phantom model REF 91800 (Standard Imaging, WI) while EBT-XD films were wrapped around the shielding at radial distances of 1.0 mm and 2.0 mm (Fig. 2b). Films were held between two concentric 3D-printed cylinders made of polylactic acid ($\rho = 1.2$ g/cm^3 – $(C_3H_4O_2)_n$) as illustrated in the inset of Fig. 2b, the interior cylinder defined the distance between the films and the shielding (1.0 mm or 2.0 mm) while the exterior cylinder (1 mm thick) held the film in position. Experimental results were compared with MC simulations that adopted a cylindrical virtual scoring grid with radial resolution of 0.025 mm, axial resolution of 0.5 mm, and angular resolution of 2°.

Experimental results were compared with MC simulations using global dose ratios considering the planned dose at 2 mm depth as the reference dose, and gamma analysis with acceptance criteria of DD/DTA (3%/1 mm).

Simulation of the virtual model of the applicator

The current model of the MAASTRO applicator (and especially the proctoscope), which we experimentally tested in this work, is still undergoing final adjustments considering different materials that would be better for sterilization, more robust and more stable to manufacture. The necessary adjustments in the final design stage aim to minimally compromise the dose distribution of the validated model.

In the final design beyond Fig. 1, instead of plastic, the shielding is encapsulated by a 0.5 mm layer of stainless steel (ANSI 304), which is the only proctoscope material (apart from the shielding). It was observed experimentally that an

applicator with a 20.8 mm diameter (shown in Fig. 1) would fit too snugly into a proctoscope with an internal diameter of 21.0 mm. Hence, the diameter of the applicator was reduced to 20.4 mm to facilitate its insertion into the proctoscope. The applicator is made of PEEK (polyether ether ketone), which requires a thicker wall (d on Fig. 1b) for stable manufacturing, bringing the maximum distance between lateral channels (Fig. 1b) from 18 mm to 17 mm.

The updated MC model of the applicator was simulated and the dose distribution scored in a rectangular virtual grid with $0.2 \times 0.2 \times 0.1$ mm^3 voxel size for a region of $60 \times 60 \times 5$ mm^3 to better evaluate dose fluctuations close to the contact surface of the applicator, and in a second grid with 0.5 mm^3 voxel size for a region of $60 \times 60 \times 40$ mm^3 to evaluate depth isodoses and dose falloff. Dose leakage was scored in a cylindrical grid around the proctoscope with radial resolution of 0.2 mm, axial resolution of 0.5 mm, and angular resolution of 2°. The extra dose leakage due to electrons generated at the metallic proctoscope was scored over cylindrical sections positioned in the region with the greatest dose leakage around the proctoscope for a radial distance ranging from 0 mm to 10 mm from the proctoscope with radial resolution of 0.2 mm.

Results

Experimental validation

Source position verification

A total of 250 dwell positions were measured during the experiment after the source path was optimized, for which 22 (8.8%) presented an absolute deviation from planned dwell position greater than 1.0 mm, with a maximum deviation of 1.2 mm for a single dwell position. Of these 22 deviations greater than 1.0 mm, 19 were from measurements from channels one and five from Fig. 3, which have the largest curvature among the channels evaluated.

Figure 3 shows the overlap of the applicator, optimized source path, planned, and measured dwell positions. The deviations between planned and measured dwell positions for the channels with lowest and greatest deviations are plotted separately.

Film dosimetry

Figure 4 shows the isodoses and global dose ratios for dose distributions measured at 1 mm, 2 mm, and 5 mm depth in solid water, for which the reference dose was 28.9, 24.8, and 16.9 Gy, respectively. The maximum distance between measured and simulated isodoses for depths of 1 mm, 2 mm, and 5 mm had local variations of up to (0.8 ± 0.2) mm, (0.9 ± 0.2) mm, and (0.7 ± 0.2) mm, respectively, for the 90% isodoses. Such deviations were more likely to appear along the y direction of Fig. 4 because this is the direction most affected by the uncertainty on the source dwell position of ±1 mm. Moreover, the slanted edge of the applicator and shielding creates a bigger space between the shielding and the applicator core along the y direction, resulting in an uncertainty position of the shielding of ±0.10 mm in the x direction and ±0.15 mm in the y direction.

The maximum deviation between measured and simulated dose distributions occurs for measurements at 1 mm depth, with global dose differences reaching 6% of the reference dose of 28.9 Gy. Nonetheless, 98.6, 99.5, and

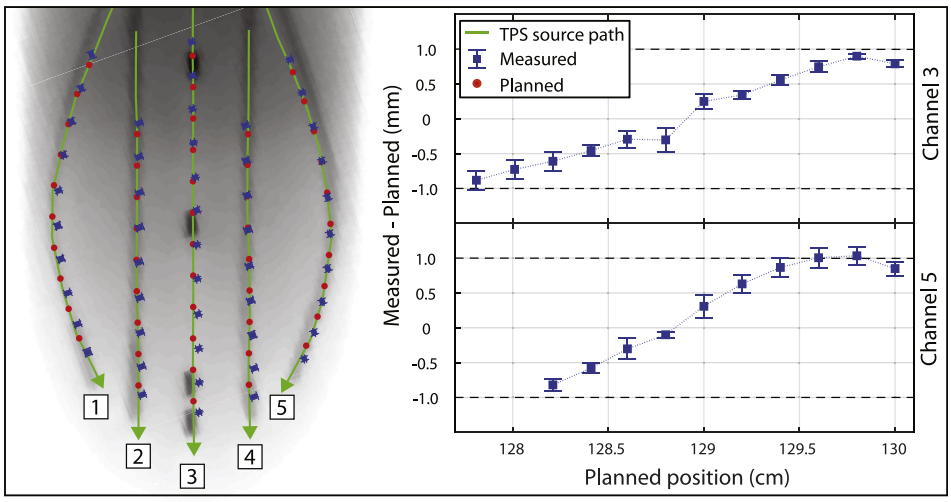

Fig. 3. Deviation between measured (IrIS) and planned dwell positions after source path optimization, which was performed by changing the source path on the TPS after each measurement until the average deviation between measured and planned dwell positions was minimized. The image on the left shows a projection of the treatment region of the applicator with dummy sources inserted into the channels (with the only purpose of highlighting the channels that were not clearly visible), as well as the optimized channel path, planned and average measured dwell position over five measurements (error bars of 2 standard deviations). The plots on the right show the deviation for channels 3 and 5, which presented the lowest and greatest deviations, respectively. IrIS = Iridium Imaging System;TPS = treatment planning system.

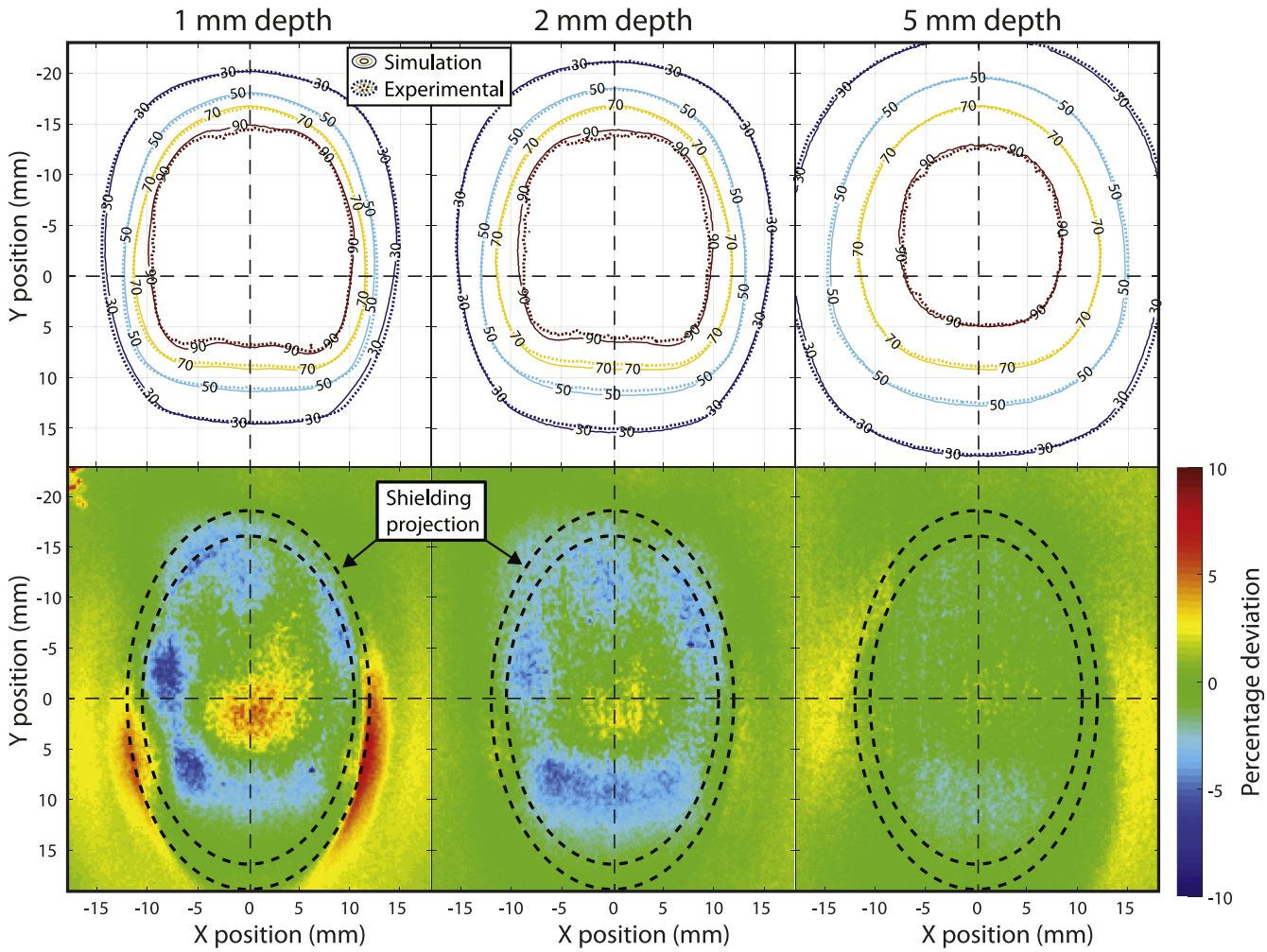

Fig. 4. Isodoses and global deviation (i.e., 100∗(Exp-Sim)/Ref. Dose) between measured and simulated dose distribution at depths of 1 mm, 2 mm, and 5 mm, adopting reference doses of 28.9, 24.8, and 16.9 Gy, respectively. Each plot has the geometric center of the contact surface adopted as reference axis (represented by vertical and horizontal dashed lines) with the same applicator orientation shown in Fig. 3.

100% of the voxels passed in a gamma analysis with acceptance criteria of DD/DTA (3%/1 mm) at depths of 1 mm, 2 mm, and 5 mm, respectively. Combined estimated uncertainties for the film measurements range from 2.2% to 7.3% (see Table 3 from Appendix), for which uncertainties type A were lower than 2%. Moreover, the uncertainty on the source position according to the afterloader manufacturer is ±1 mm (24). Hence, the acceptance criteria of DD/DTA (3%/1 mm) were chosen to be conservative.

The gamma analysis for the dose leakage experiment measured at radial distance of 1 mm and 2 mm from the shielding resulted in 96.8% and 94.7% of the voxels passing acceptance criteria of DD/DTA (3%/1 mm), and maximum global dose ratios of 5.4% and 4.2%, respectively, for a reference dose of 24.8 Gy (planned dose at 2 mm depth).

Simulation of the virtual model of the applicator

Figure 5a shows that the center of the simulated dose distribution at 2 mm depth (intersection between lines L2 and L3) is at a distance of 5.2 ± 0.2 mm from the geometric center of the contact surface (intersection between lines L1 and L2). This follows from the design of the applicator (as shown in Design of the MAASTRO applicator Section) where the slanted edge does not allow dwell positions close to the edge of the contact surface at the most distal end of the applicator, as shown in Fig. 1c. Nevertheless, such a shift is constant for all depths evaluated, as shown by the dose profiles and isodoses along line L2 (Figs. 5c and 5d). The 90% isodose at 2 mm depth covers a region of (21.6 ± 0.2) mm along line L2 and 18.2 ± 0.2 mm along line L3.

The resulting dose falloff scored at the center of the dose distribution (Fig. 5b) is slightly steeper than the one produced by the P50 device with a 22 mm applicator (8). Normalized at 2 mm, the dose falloff for depths of 0, 5, and 10 mm are 130%, 70%, and 43% for the P50 with a 22 mm applicator and 140%, 67%, and 38% for the MAASTRO applicator, respectively. CXB treatments usually prescribe a surface dose of 30 Gy (10,11), meaning that 23.1 Gy would be delivered at 2 mm depth according to

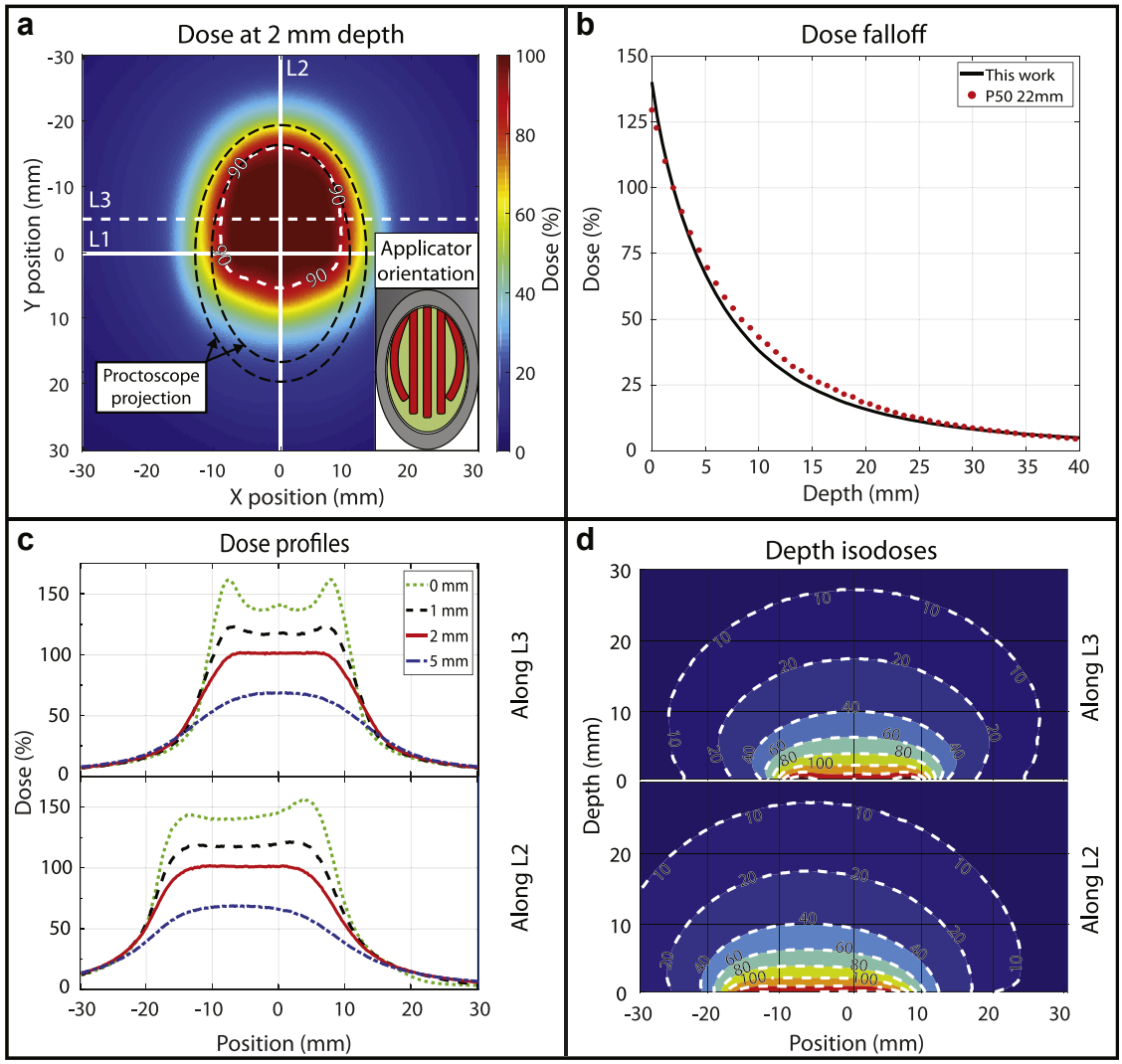

Fig. 5. Simulated dose distribution for the MAASTRO applicator with the geometric center of the contact surface adopted as reference axis. (a) Dose distribution at 2 mm depth showing the geometric center of the contact surface (intersection between lines L1 and L2), the center of the dose distribution (intersection between lines L2 and L3) and the 90% isodose; (b) Dose falloff along the center of the dose distribution compared to the dose falloff of the Papillon 50 device with a 22 mm applicator; (c) Dose profiles at 0 mm, 1 mm, 2 mm, and 5 mm depths along lines L2 and L3 and, (d) Depth isodoses along lines L2 and L3.

the P50 dose falloff used as reference. The MAASTRO applicator can deliver 23.1 Gy at 2 mm depth in approximately 3 min of irradiation time using a 40700 U (10 Ci) source or 6 min with a 20350 U (5 Ci) source. Nevertheless, the time required to perform obstruction verifications (dummy checks) with the GammaMedplus iX afterloader is approximately 30 s per channel, which increases the treatment time (irradiation + dummy check) by 2.5 min for the MAASTRO applicator. The P50 surface dose rate ranges from 20 to 35 Gy/min depending on the applicator adopted (9), resulting in a irradiation time of less than 1 min and 30 s for the applicator with lowest dose rate (30 mm applicator).

Simulated dose profiles at 0 mm, 1 mm, 2 mm, and 5 mm depths along lines L2 and L3 (Fig. 5c), show that the surface dose is not uniform (oscillating along line L3 between 136% and 160% of the reference dose at 2 mm depth); however, such fluctuation is reduced between 123% and 117% at 1 mm depth.

The dose leakage for a 0.2 mm-thick layer around the proctoscope (Fig. 6) is greater close to the two channels adjoining the edges of the treatment surface with maximum leakage hotspots reaching 49% of the planned dose at 2 mm (hotspots are indicated by arrows in Fig. 6). Nevertheless, the dose leakage quickly drops to less than 30% (less than 7 Gy for a typical CXB treatment) for regions that are 5 mm or further from the contact surface (distance pointed by the dashed arrow in Fig. 6). These dose values, however, do not include the extra dose from secondary electrons generated in the proctoscope. The leakage dose for regions with 30% leakage or more are, on average, increased by 9% (i.e., 30% leakage will become 32.7%) because of secondary electrons for the first 0.2 mm layer around the proctoscope. The electron contribution to the leakage dose drops, however, from 9% to less than 1% (becoming negligible) when dose is scored between 0.6 mm and 0.8 mm from the proctoscope.

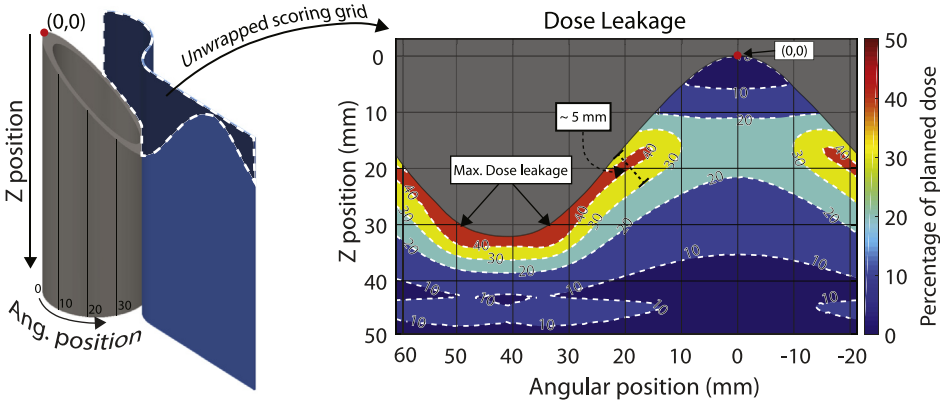

Fig. 6. Simulated dose leakage around the proctoscope for a 0.2 mm-thick cylindrical scoring grid. The cylinder with a slanted edge shows how the scoring grid was wrapped around the proctoscope, having the sharp edge of the proctoscope adopted as reference position (0,0) for the scoring grid. The region above the proctoscope edge was masked for better evaluation of dose leakage through the proctoscope wall.

Discussion

The MAASTRO applicator was evaluated with two series of experimental validations to verify the dwell position accuracy and dosimetry. This was followed by MC simulations of the virtual (CAD) model of the applicator to characterize the dose distribution expected for the final manufactured product.

Experimental validation

Source position verification

Local deviations between measured and planned dwell positions for curved applicators are well known and reported in the literature (6,25,26). Nevertheless, the average absolute deviation between measured and planned dwell positions after source path optimization for the channels with the highest deviations (one and five from Fig. 3) was (avg. (range)) 0.7 (0.1−1.2) mm and the average absolute deviation for the remaining channels was 0.5 (0.0−1.1) mm, showing no relevant statistical difference among channels after the applicator was properly commissioned (18). Moreover, the deviations between measured and planned dwell positions are within the afterloader precision of ±1.0 mm (24).

Film dosimetry

Local discrepancies between MC simulations and experiments with film dosimetry reach a maximum of 6% at 1 mm depth close to the shielding (see Fig. 4). Such local deviation is believed to be due to a small shift in the shielding position or inclination that could have a large impact on the local dose distribution at 1 mm depth because it is a region of steep dose gradient. Nevertheless, the region affected by the shielding passes the gamma analysis while the points that fail the gamma analysis are in the treatment region, indicating that the uncertainty on the distance between the source and the scoring plane plays a bigger role on the overall dose distribution. Nevertheless, such variations are not clinically relevant because the first few millimeters of the tumor will be removed after each fraction anyway.

Simulation of the virtual model of the applicator

Simulations show that the MAASTRO applicator can generate a radiation field suitable for treatment of small rectal tumors, presenting a steep dose falloff similar to those of 50 kVp CXB devices. However, the contact surface of the applicator has a cold region that must be accounted for. For this reason, the proctoscope will have clearly visible engravings to guide its placement against the tumor considering the high- and low-dose regions of the contact surface.

The longer treatment time for the MAASTRO applicator (8 min and 30 s using a 20350 U source) is acceptable for a BT treatment; however, it will require extra care to safeguard that the applicator will not move during the irradiation.

The greater (when compared to P50) and heterogeneous surface dose distribution is unlikely to jeopardize a treatment outcome because experiences with the P50 device show that the first few millimeter of the tumor are removed after each fraction (10), and P50 delivers a surface dose greater than 30 Gy for tumors that protrude into the applicator (27). Moreover, the relatively wide beam aperture (Figs. 5c and 5d) may be beneficial to treat microscopic residual tumors, which extends from the gross tumor by 4.7 mm on average (28). Moreover, a study by Reniers et al. (29), has reported that 50 kVp x-rays emitted by an Axxent (Xoft Inc., CA) electronic BT source may have a biological effect approximately 40% higher than the photons from an HDR ^{192}Ir source. However, clinical studies are necessary to evaluate such effects.

Conclusion

The MAASTRO applicator was specifically designed to deliver a high surface dose (>30 Gy) in less than 10 min (even with a low air-kerma strength—20350 U) to a small

target region of $\approx 20 \times 20$ mm^2 while sparing OAR surrounding the applicator. This is an advantage compared with external beam radiotherapy boosting techniques, where the high-dose region is less localized, resulting in greater toxicity (4). Such dose distribution required a complex multichannel arrangement bringing the source close and parallel to the treatment surface while OAR are protected by lateral shielding. Unlike most BT applicators, the MAASTRO applicator uses the inverse square law to achieve a steep dose falloff by bringing the HDR ^{192}Ir source in close contact to the tumor in multiple points, whereas CXB devices, such as the P50 and the Xoft eBT rectal applicator (30), rely on 50 kVp x-rays to achieve a similar result. The MAASTRO applicator was developed to be used with commonly available HDR ^{192}Ir BT sources, which allows it to be used with regular HDR afterloaders already available in most oncology centers without the need for extra equipment, differently from CXB devices that require a 50 kVp x-rays source. Furthermore, the applicator is compatible with currently available TPSs allowing patient-specific dose distributions. For these reasons, the MAASTRO applicator holds the potential of being a cost-effective solution for endoluminal boosting in radiotherapy.

Acknowledgments

M.B. was partially supported by a scholarship from CNPq, Conselho Nacional de Desenvolvimento Científico e Tecnológico—Brazil, grant number 200402/2015-3.

Supplementary data

Supplementary data related to this article can be found at https://doi.org/10.1016/j.brachy.2020.03.009.

References

[1] Siegel RL, Miller KD, Jemal A. Cancer statistics, 2019. *CA Cancer J Clin* 2019;69:7–34.
[2] Konanz J, Herrle F, Weiss C, *et al*. Quality of life of patients after low anterior, intersphincteric, and abdominoperineal resection for rectal cancer–a matched-pair analysis. *Int J Colorectal Dis* 2013;28:679–688.
[3] Appelt AL, Ploen J, Vogelius IR, *et al*. Radiation dose-response model for locally advanced rectal cancer after preoperative chemoradiation therapy. *Int J Radiat Oncol Biol Phys* 2013;85:74–80.
[4] Gerard JP, Frin A-C, Doyen J, *et al*. Organ preservation in rectal adenocarcinoma (T1) T2-T3 Nx M0. Historical overview of the Lyon Sud – nice experience using contact x-ray brachytherapy and external beam radiotherapy for 120 patients. *Acta Oncol* 2015;54:550–556.
[5] Bellezzo M, Fonseca GP, Verrijssen AS, *et al*. A novel rectal applicator for contact radiotherapy with HDR (192)Ir sources. *Brachytherapy* 2018;17:1037–1044.
[6] Kirisits C, Rivard MJ, Baltas D, *et al*. Review of clinical brachytherapy uncertainties: Analysis guidelines of GEC-ESTRO and the AAPM. *Radiother Oncol* 2014;110:199–212.
[7] Elfrink RJM, Kolkman-Deurloo I-KK, van Kleffens HJ, *et al*. Determination of the accuracy of implant reconstruction and dose delivery in brachytherapy in The Netherlands and Belgium. *Radiother Oncol* 2001;59:297–306.
[8] Croce O, Hachem S, Franchisseur E, *et al*. Contact radiotherapy using a 50kV X-ray system: Evaluation of relative dose distribution with the Monte Carlo code PENELOPE and comparison with measurements. *Radiat Phys Chem* 2012;81:609–617.
[9] Sun Myint A. Renaissance of contact radiotherapy with RT 50 papillon machine: Preliminary data on first 100 patients treated at Clatterbridge. *J Clin Oncol* 2011;29:e14149.
[10] Sun Myint A, Stewart A, Mills J, *et al*. Treatment: The role of contact X-ray brachytherapy (Papillon) in the management of early rectal cancer. *Colorectal Dis* 2019;21:45–52.
[11] Sun Myint A, Wong H, Whitmarsh K, *et al*. Dose escalation using contact X-ray brachytherapy (Papillon) for rectal cancer: Does it improve the chance of organ preservation? *Br J Radiol* 2017;90(1080):20170175.
[12] Goorley T, James M, Booth T, *et al*. Features of MCNP6. *Ann Nucl Energy* 2016;87:772–783.
[13] Nath R, Anderson LL, Luxton G, *et al*. Dosimetry of interstitial brachytherapy sources: Recommendations of the AAPM radiation therapy committee task group No. 43. *Med Phys* 1995;22:209–234.
[14] Perez-Calatayud J, Ballester F, Das RK, *et al*. Dose calculation for photon-emitting brachytherapy sources with average energy higher than 50 keV: Report of the AAPM and ESTRO. *Med Phys* 2012;39:2904–2929.
[15] Fonseca GP, Tedgren AC, Reniers B, *et al*. Dose specification for 192Ir high dose rate brachytherapy in terms of dose-to-water-in-medium and dose-to-medium-in-medium. *Phys Med Biol* 2015;60:4565–4579.
[16] Williamson JF. Monte Carlo evaluation of kerma at a point for photon transport problems. *Med Phys* 1987;14:567–576.
[17] Scapin M. Mechanical characterization and modeling of the heavy tungsten alloy IT180. *Int J Refract Metals Hard Mater* 2015;50:258–268.
[18] Fonseca GP, Van den Bosch MR, Voncken R, *et al*. A novel system for commissioning brachytherapy applicators: Example of a ring applicator. *Phys Med Biol* 2017;62:8360–8375.
[19] EBT-XD specification and user guide. Available at: http://www.gafchromic.com/documents/EBTXD_Specifications_Final.pdf. Accessed July 1, 2019.
[20] Micke A, Lewis DF, Yu X. Multichannel film dosimetry with nonuniformity correction. *Med Phys* 2011;38:2523–2534.
[21] Grams MP, Gustafson JM, Long KM, *et al*. Technical note: Initial characterization of the new EBT-XD gafchromic film. *Med Phys* 2015;42:5782–5786.
[22] Low DA, Harms WB, Mutic S, *et al*. A technique for the quantitative evaluation of dose distributions. *Med Phys* 1998;25:656–661.
[23] Low DA, Dempsey JF. Evaluation of the gamma dose distribution comparison method. *Med Phys* 2003;30:2455–2464.
[24] *GammaMedplus™ iX instructions for use including the GammaMedplus™ 3/24 iX*. Palo Alto, CA: Varian Medical Systems; 2018.
[25] Bellezzo M, Baeza JA, Voncken R, *et al*. Mechanical evaluation of the Bravos afterloader system for HDR brachytherapy. *Brachytherapy* 2019;18:852–862.
[26] Stern RL, Liu T. Dwell position inaccuracy in the Varian GammaMed HDR ring applicator. *J Appl Clin Med Phys* 2010;11:3158.
[27] Myint AS, Gerard JP. Minimally invasive contact X-ray brachytherapy as an alternative option in patients with rectal cancer not suitable for bespoke surgical resection. *Minim Invasive Surg* 2018;2(10):34.
[28] Verrijssen A, Bellezzo M, Habr-Gama A, *et al*. EP-1472: Microscopic extension of residual rectal tumor mass post-neoadjuvant chemoradiation: a meta-analysis. *Radiother Oncol* 2018;127:S799.
[29] Reniers B, Liu D, Rusch T, *et al*. Calculation of relative biological effectiveness of a low-energy electronic brachytherapy source. *Phys Med Biol* 2008;53:7125–7135.
[30] Liang LH, Tomic N, Vuong T, *et al*. Physics aspects of the Papillon technique-Five decades later. *Brachytherapy* 2018;17:234–243.